electronic materials

MDPI

Article

Calculation of Band Offsets of $Mg(OH)_2$-Based Heterostructures

Masaya Ichimura

Department of Electrical and Mechanical Engineering, Nagoya Institute of Technology, Nagoya 466-8555, Japan; ichimura.masaya@nitech.ac.jp

Abstract: The band alignment of $Mg(OH)_2$-based heterostructures is investigated based on first-principles calculation. (111)-MgO/(0001)-$Mg(OH)_2$ and (0001)-wurtzite ZnO/(0001)-$Mg(OH)_2$ heterostructures are considered. The O 2s level energy is obtained for each O atom in the heterostructure supercell, and the band edge energies are evaluated following the procedure of the core-level spectroscopy. The calculation is based on the generalized gradient approximation with the on-site Coulomb interaction parameter U considered for Zn. For MgO/$Mg(OH)_2$, the band alignment is of type II, and the valence band edge of MgO is higher by 1.6 eV than that of $Mg(OH)_2$. For ZnO/$Mg(OH)_2$, the band alignment is of type I, and the valence band edge of ZnO is higher by 0.5 eV than that of $Mg(OH)_2$. Assuming the transitivity rule, it is expected that $Mg(OH)_2$ can be used for certain types of heterostructure solar cells and dye-sensitized solar cells to improve the performance.

Keywords: $Mg(OH)_2$; heterostructure; band alignment; first-principles calculation

Citation: Ichimura, M. Calculation of Band Offsets of $Mg(OH)_2$-Based Heterostructures. *Electron. Mater.* **2021**, 2, 274–283. https://doi.org/10.3390/electronicmat2030019

Received: 11 June 2021
Accepted: 26 June 2021
Published: 1 July 2021

1. Introduction

Magnesium hydroxide $Mg(OH)_2$ has normally been regarded as an insulator and its applications have been limited in chemistry fields so far. However, there were several attempts to apply $Mg(OH)_2$ to solar cells. It was reported that the performance of dye-sensitized solar cells (DSSC) was improved by an $Mg(OH)_2$ coating on the TiO_2 particles [1,2]. $Mg(OH)_2$ was also used for a buffer layer of $Cu(InGa)Se_2$ (CIGS)-based heterostructure solar cells [3,4]. The most common buffer-layer material is CdS, but Cd is toxic and not abundant. In contrast, Mg is nontoxic and earth-abundant, thus $Mg(OH)_2$ is advantageous for domestic solar cell application.

In those electronics application, if $Mg(OH)_2$ is completely insulating, devices do not work. Thus, the successful applications to solar cells indicate that $Mg(OH)_2$ has some conductivity. $Mg(OH)_2$ has a wide bandgap of 5.7 eV [5,6], but materials having a comparable bandgap have begun to be used in electronics as ultra-wide bandgap (UWBG) semiconductors. For example, diamond, with a bandgap that is similar to that of $Mg(OH)_2$, has been extensively investigated for electronic device applications. Ga_2O_3, with a bandgap of approximately 5 eV, has also attracted much attention, and $(Al_xGa_{1-x})_2O_3$, having a bandgap even larger than that of Ga_2O_3, is considered to be indispensable for heterostructure devices based on Ga_2O_3. Thus, it is natural to consider $Mg(OH)_2$ as another UWBG semiconductor. It was reported that chemically deposited $Mg(OH)_2$ (nominally undoped) is semiconducting [7], and that Cu-doped $Mg(OH)_2$ fabricated by electrochemical deposition can have both n-type and p-type conductivity depending on fabrication conditions [8–10]. Recently, the first-principles calculation was carried out to evaluate impurity and defect levels and to discuss the possibility of controlling the conduction type and conductivity of $Mg(OH)_2$ [11]. In addition, the possibility of bandgap reduction by anion doping has been theoretically investigated [12]. It was also reported that resistivity was much reduced, to the order of 10^{-2} Ω cm, by heavy carbon doping [13,14].

Additional essential information for designing the heterostructure devices is band alignment. To analyze the performance of both DSSC and heterostructure solar cells includ-

ing an $Mg(OH)_2$ layer, one needs to consider carrier transport across the heterointerface with $Mg(OH)_2$. The band alignment critically influences the carrier transport across the heterointerface. For many kinds of semiconductor heterostructures, band alignment has been investigated. The core-level spectroscopy is the most popular technique for evaluating the band offset experimentally [15–18]. Theoretical research has also been carried out for various heterostructures. Recently, band structures of two-dimensional (2D) heterostructures based on $Mg(OH)_2$ were theoretically investigated for various partners [19–22]. In those previous works, only 2D $Mg(OH)_2$ (a single monolayer of $Mg(OH)_2$) was considered, and the interface bonding was assumed to be due to the van der Waals interaction. To my knowledge, the band alignment of heterostructures based on bulk $Mg(OH)_2$ (with covalent bonding at the interface) has not been investigated so far.

In this work, band alignment at the $Mg(OH)_2$-based heterostructures is investigated by first-principles calculations. MgO and ZnO are selected as the partner of the heterostructure. MgO has the NaCl structure, and ZnO the wurtzite structure. The arrangement of oxygen atoms in the (111) plane of MgO and (0001) plane of ZnO is the same as that of (0001) plane of $Mg(OH)_2$. Thus, one can construct heterointerfaces with an $Mg(OH)_2$ (0001) plane. ZnO is a popular buffer layer material of heterostructure solar cells, and band alignment has been investigated for various heterostructures based on ZnO. Therefore, once the band offset with ZnO was evaluated, band offset could be estimated for other heterostructures with various materials by assuming the transitivity rule [17,18].

2. Calculation

The supercells used in the calculation are shown in Figure 1. The hetero-interface is (111) plane for MgO (Figure 1a) and (0001) plane for wurtzite ZnO (Figure 1b). The lattice constant parallel to the interface was fixed at the average of the constituent compounds, weighted by the respective thickness, and the vertical atom spacings were initially set the same as that of the respective compound. All of the atoms are allowed to relax with the supercell size fixed. The GDIIS (geometry optimization by direct inversion in the iterative subspace) algorism was adopted [23], and the convergence criterion was 5×10^{-2} eV/Å. (The lattice constants and atom positions after relaxation are given in Tables A1 and A2.)

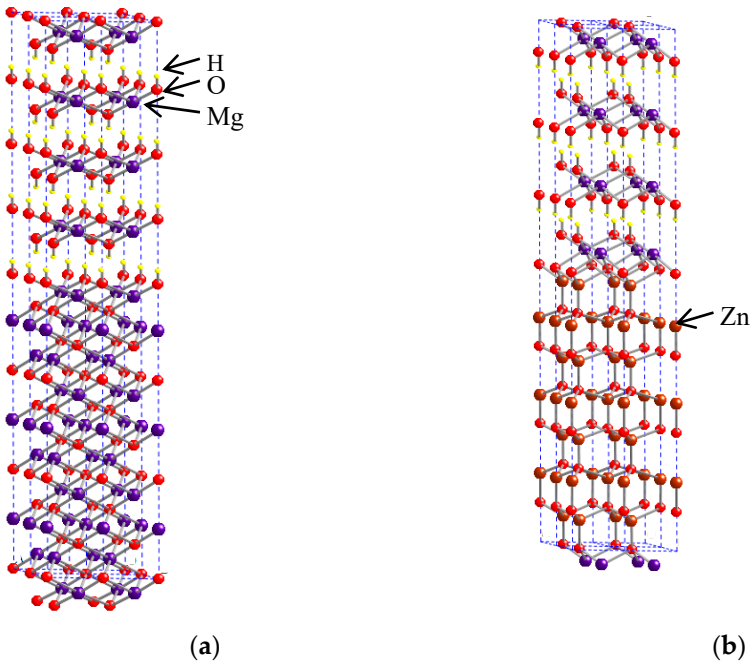

Figure 1. (**a**) MgO/$Mg(OH)_2$ and (**b**) ZnO/$Mg(OH)_2$ supercells used in the calculation.

MgO has the NaCl structure, and the lattice is fcc. Thus, the atom stacking of (111) plane is denoted as ABC, where A, B, and C represent different atom positions. For $Mg(OH)_2$, the atom position is the same for each OH-Mg-OH monolayer, and the stacking of O atom planes can be denoted as ACAC. In the supercell of $MgO/Mg(OH)_2$, the thickness of MgO is set at 9-monolayers and that of $Mg(OH)_2$ is 4 monolayers, and the stacking of O atoms is as follows:

$$\underline{ABCABCABC}\underline{ACACACAC}$$
$$MgO \qquad Mg(OH)_2$$

As shown in Figure 1a, the Mg atom at the interface is bonded to O atoms on the MgO side and the OH groups on the $Mg(OH)_2$ side. The unstrained O-O distance is 0.297 nm for MgO and 0.314 nm for $Mg(OH)_2$, and thus the lattice mismatch is not very large.

ZnO has the wurtzite structure, and its lattice is hcp, with ABAB atom stacking along [0001]. In the supercell of $ZnO/Mg(OH)_2$, to avoid energetically unfavorable stacking (such as AA) and to keep periodicity, the ZnO thickness was set at 7 monolayers. The stacking of O atoms is as follows:

$$\underline{BABABABA}\underline{BABABABA}\underline{B}$$
$$ZnO \qquad Mg(OH)_2$$

The underlined atoms correspond to the interface and are bonded to both Zn and Mg (O-Zn-O-Mg-O-H), as shown in Figure 1b. In fact, for this heterostructure, one can consider two types of interfaces: one is the oxide-like interface where the atoms are stacked as Zn-O-Mg, and the other is the hydroxide-like interface where the atom stacking is Zn-O-H-H-O-Mg. Since zinc hydroxide is not stable when close to room temperature, we assume the oxide-like interface. The lattice mismatch is not large for the $ZnO/Mg(OH)_2$ heterostructure either because the atom spacing in the (0001) plane of unstrained ZnO is 0.325 nm.

The calculation in this work is based on the density-functional theory (DFT) [24,25]. PHASE code (ver.11.0, University of Tokyo, Tokyo, Japan) was used. The pseudopotential method was adopted with generalized-gradient approximation (GGA) of ref. [26]. The ultrasoft pseudopotentials were used for O and Zn, and the norm-conserving pseudopotentials for H and Mg. The kinetic energy cutoff of the basis set was 272 eV (20 Rydberg). The effects of the on-site Coulomb interaction U for d states of Zn were included in the calculation (GGA + U), using the value of U = 5.0 eV [27,28].

The band offset was evaluated by a procedure similar to the core-level spectroscopy. The local density of states was obtained for each constituent atom in the supercell, and the O 2s level was used as the inner core level. It was assumed that the difference between the O 2s level and the valence band maximum E_v is preserved. It is known that the bandgap is underestimated by the DFT calculation [29]; the calculated bandgap of $Mg(OH)_2$ is approximately 4 eV, considerably smaller than the experimental value (5.7 eV). Thus, the energy of the conduction band minimum E_c was determined from the calculated E_v and the experimentally determined bandgap.

3. Results and Discussion

The energies of O 2s are plotted in Figure 2 for the O atoms in the $MgO/Mg(OH)_2$ supercell (the squares). The O 2s level is lower in $Mg(OH)_2$ than in MgO by approximately 2.8 eV. It was reported that the binding energy of O 1s obtained in X-ray photoelectron spectroscopy (XPS) is larger in $Mg(OH)_2$ than in MgO by 1.8 eV [30,31]. Thus, the XPS results also indicate that the O levels are lower in energy in $Mg(OH)_2$ than in MgO. The band edge energies E_v and E_c are also plotted in Figure 2. The bandgap of MgO is considered to be 7.8 eV [32,33]. The band alignment is of type II, i.e., both E_c and E_v are lower in energy in $Mg(OH)_2$.

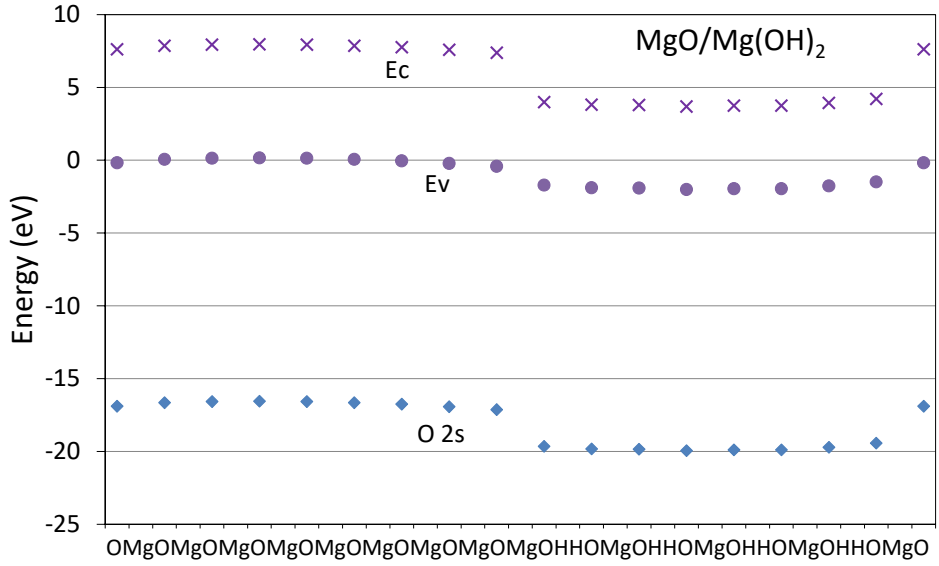

Figure 2. Calculated O 2s levels in $MgO/Mg(OH)_2$, and the band edge energies E_v and E_c evaluated by the procedure of the core-level spectroscopy.

The O 2s level and the band edge energies in the $ZnO/Mg(OH)_2$ supercell are plotted in Figure 3. (0001) of wurtzite is a polar face, and in Figure 3, the center of the figure corresponds to the O-face of ZnO. The slope in the energy levels indicates the presence of a macroscopic electric field with a net positive charge at the center of the figure owing to the polarization in ZnO. Because of the slope, it is difficult to rigorously define the band edge position; we take the average of E_v and E_c in the respective layer and estimate the band offset, then the valence band offset ΔE_v is 0.5 eV with E_v of ZnO is higher.

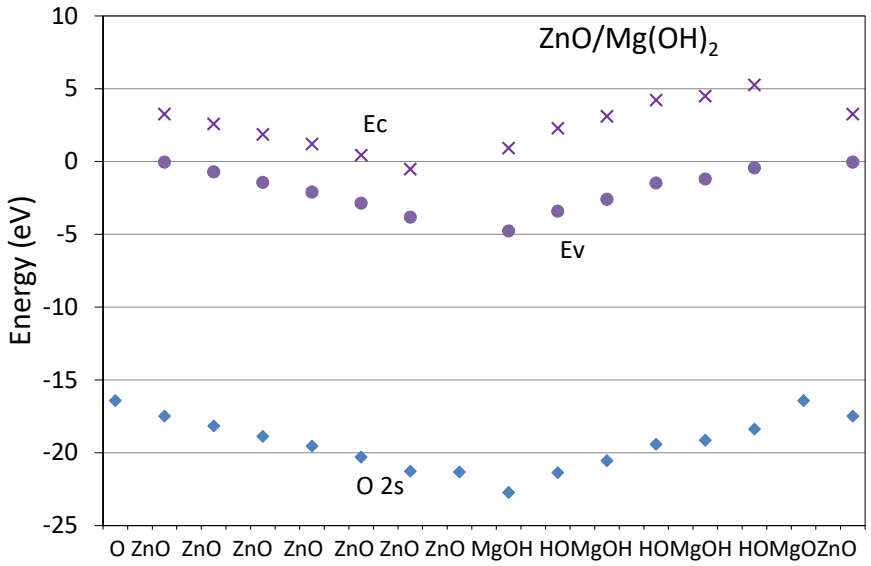

Figure 3. Calculated O 2s levels, E_v, and E_c in $ZgO/Mg(OH)_2$ evaluated by the procedure of the core-level spectroscopy.

The results are summarized in Figure 4. E_v of MgO is positioned at a higher energy than E_v of $Mg(OH)_2$, and MgO has a larger bandgap. Thus, for $MgO/Mg(OH)_2$, the band alignment is of type II, and the conduction band offset ΔE_c is very large. On the other

hand, for ZnO/$Mg(OH)_2$, the band alignment is of type-I, with a larger band offset for the conduction band side.

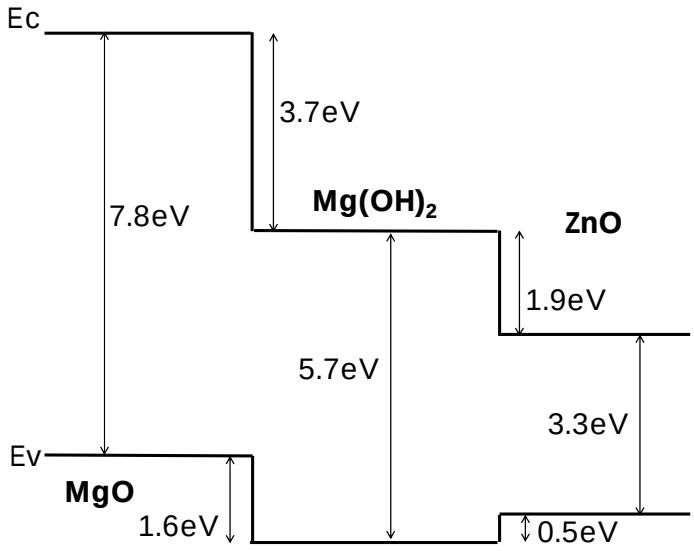

Figure 4. Band alignment for MgO/$Mg(OH)_2$ and ZgO/$Mg(OH)_2$ heterointerfaces.

As noted in the introduction, CdS is the most common buffer-layer material in CIGS-based heterostructure solar cells, but Cd is toxic and not abundant. ZnO has been considered as an alternative buffer-layer material. In the ZnO/CIGS heterostructure, the band alignment is of type-II and the E_c of ZnO is lower by 0.16 eV [34,35]. Lower E_c in the buffer layer reduces band bending, and increases the recombination of the majority of carriers, decreasing output voltage. Thus, it is expected that alloying with MgO could shift the E_c of ZnO upward and improve solar-cell performance [36]. Alternatively, assuming the transitivity rule, the band alignment is of type-I for $Mg(OH)_2$/CIGS, and thus higher output voltage can be expected than for ZnO/CIGS. However, ΔE_c at $Mg(OH)_2$/CIGS may be too large (about 1.7 eV) so output current would be reduced. In fact, in ref. [4], the efficiency of an $Mg(OH)_2$/CIGS solar cell was reported as low. ZnO/Cu_2O is another heterostructure attracting attention for solar cell application. It is generally agreed that the band alignment is of type-II, although different values of band offsets were reported (the reported values of ΔE_c range from 0.5 and 1.77 eV) [37–39]. Thus, to improve performance, oxides with a larger bandgap (such as $Zn_{1-x}Mg_xO$ and Ga_2O_3) have been employed, so that its E_c becomes higher than the E_c of Cu_2O [39,40]. According to the present calculation, E_c of $Mg(OH)_2$ is positioned significantly higher than that of ZnO. Then, the replacement of ZnO with $Mg(OH)_2$ in the Cu_2O-based solar cell will result in the type-I band alignment with moderate ΔE_c value and thus could increase output voltage and power.

$Mg(OH)_2$ has been used for the coating of TiO_2 in DSSC, as noted in the introduction [1,2]. In DSSC, photo-excited electrons are injected from dye to TiO_2, but a part of those electrons are lost because of the backflow to the dye or ions in the electrolyte. It is known that the band offset between ZnO and TiO_2 is small for both of the bands [41–43]. Thus, the band offset at $Mg(OH)_2/TiO_2$ will be similar to that at $Mg(OH)_2$/ZnO, according to the transitivity rule. Then, ΔE_c at $Mg(OH)_2/TiO_2$ could be large, and therefore, the $Mg(OH)_2$ coating will block the backflow of photo-generated electrons from TiO_2, increasing the output. However, it may also prevent the injection of electrons from the dye to TiO_2. According to the previous works, a thin $Mg(OH)_2$ coating on TiO_2 led to an increase in output voltage without significant a decrease in the output current, but thicker coatings resulted in a decrease in the current and efficiency. Since LUMO (energy of excited electrons) in the dye is higher than E_c of TiO_2, the energy barrier of the $Mg(OH)_2$ coating is smaller for the carrier injection from the dye than for the backflow from TiO_2. Thus, if the $Mg(OH)_2$ coating thickness is properly adjusted, it could block the backflow from TiO_2

without significantly blocking the carrier injection from the dye, leading to an increase in photovoltaic output.

It should be noted that the calculation based on a small supercell will not be applicable for the heterostructure with Cu_2O or TiO_2 because of a different arrangement of O atoms. Thus we have discussed the properties of those heterostructures based on the transitivity rule. However, the rule does not hold when the effects of the interface dipole are significant. For more conclusive discussion, the band offset needs to be experimentally measured.

In the present calculation, a perfect interface without any defects was assumed. For $Mg(OH)_2$, a cation (Mg) vacancy is expected to act as an acceptor, and an anion (OH) vacancy as a donor, as for metal oxides [11]. Another possible disorder is the inclusion of the hydroxide-like interface (e.g., Zn-O-H-H-O-Mg). The defects at the interface could modify the charge distribution near the interface and affect the band alignment. However, it is difficult to predict the effects of those disorders, to take into account those effects in the calculation, a much larger supercell needs to be used.

Finally, the present results are compared with the theoretical results for the 2D $ZnO/Mg(OH)_2$ heterostructure by Ren et al. [22]. They predicted the type-II band alignment for $ZnO/Mg(OH)_2$ with E_v of ZnO lower than that of $Mg(OH)_2$ while the type-I alignment was predicted in the present work. In their calculation, 2D ZnO was considered, i.e., Zn and O atoms were arranged on a single atom plane. Thus, the bonding configuration is different from the tetrahedral bonding in actual bulk ZnO. This could be the main reason for the qualitative discrepancy.

For $Mg(OH)_2$ to be applied to devices, control of conduction type, and conductivity will be necessary. Although there are some preliminary attempts of valence control of $Mg(OH)_2$ as noted in the introduction [8–11], doping techniques need to be established for the device application.

4. Conclusions

The band alignment of the $Mg(OH)_2$-based heterostructures was investigated based on the first-principles calculation. The O 2s level energy was obtained for each O atom in the heterostructure supercell, and the band edge energies were evaluated following the procedure of the core-level spectroscopy. For $MgO/Mg(OH)_2$, the band alignment is of type II, and the E_v of MgO is higher by 1.6 eV than that of $Mg(OH)_2$. The band alignment of $ZnO/Mg(OH)_2$ is of type I, and ΔE_v is 0.5 eV. Assuming the transitivity rule, it is expected that $Mg(OH)_2$ can increase the output voltage of the heterostructure solar cells and DSSC if its thickness is properly adjusted.

Funding: This research received no external funding.

Institutional Review Board Statement: Not applicable.

Informed Consent Statement: Not applicable.

Data Availability Statement: The data presented in this study are available on request from the corresponding author.

Conflicts of Interest: The author declares no conflict of interest.

Appendix A

The structure of the supercells. Both of the supercells are hexagonal, and the lattice constants and atom positions after the relaxation (internal coordinate) are as follows:

Table A1. $MgO/Mg(OH)_2$, a = b = 3.054 Å, c = 40.950 Å.

O	−0.0002	0.0000	0.0002
Mg	0.6661	0.3330	0.0297
O	0.3330	0.6661	0.0594
Mg	−0.0002	−0.0002	0.0890
O	0.6661	0.3330	0.1187
Mg	0.3330	0.6662	0.1484
O	−0.0001	−0.0001	0.1781
Mg	0.6662	0.3330	0.2078
O	0.3330	0.6661	0.2375
Mg	−0.0002	−0.0002	0.2672
O	0.6661	0.3330	0.2969
Mg	0.3330	0.6662	0.3266
O	−0.0001	−0.0001	0.3563
Mg	0.6661	0.3330	0.3860
O	0.3330	0.6661	0.4156
Mg	−0.0001	−0.0001	0.4453
O	0.6663	0.3330	0.4748
Mg	0.3332	0.6666	0.5044
O	−0.0002	0.0001	0.5296
H	0.0000	0.0000	0.5531
H	0.6667	0.3333	0.5724
O	0.6669	0.3331	0.5958
Mg	0.3333	0.6666	0.6212
O	−0.0002	0.0001	0.6464
H	0.0000	0.0000	0.6698
H	0.6667	0.3333	0.6888
O	0.6668	0.3331	0.7122
Mg	0.3333	0.6666	0.7375
O	−0.0001	0.0001	0.7628
H	0.0000	0.0000	0.7862
H	0.6667	0.3333	0.8052
O	0.6668	0.3331	0.8286
Mg	0.3333	0.6666	0.8539
O	−0.0002	0.0002	0.8792
H	0.0000	0.0000	0.9026
H	0.6667	0.3333	0.9219
O	0.6668	0.3332	0.9455
Mg	0.3333	0.6666	0.9706

Table A2. $ZnO/Mg(OH)_2$, a = b = 3.198 Å, c = 34.645 Å.

O	0.6623	0.3372	−0.0020
Zn	0.6636	0.3360	0.0525
O	0.0033	−0.0038	0.0753
Zn	−0.0004	−0.0001	0.1312
O	0.6656	0.3339	0.1513
Zn	0.6666	0.3329	0.2073
O	−0.0003	−0.0002	0.2265
Zn	−0.0007	0.0002	0.2823
O	0.6664	0.3331	0.3014
Zn	0.6666	0.3330	0.3569
O	−0.0007	0.0003	0.3753
Zn	0.0000	−0.0007	0.4303

Table A2. *Cont.*

O	0.6677	0.3317	0.4483
Zn	0.6646	0.3349	0.5027
O	−0.0001	−0.0006	0.5319
Mg	0.3325	0.6671	0.5663
O	0.6660	0.3336	0.5917
H	0.6670	0.3328	0.6198
H	0.0001	−0.0001	0.6371
O	−0.0002	0.0001	0.6648
Mg	0.3333	0.6667	0.6957
O	0.6669	0.3331	0.7236
H	0.6668	0.3332	0.7515
H	0.0000	0.0000	0.7745
O	−0.0002	0.0002	0.8022
Mg	0.3333	0.6667	0.8332
O	0.6669	0.3331	0.8609
H	0.6668	0.3331	0.8889
H	0.0002	−0.0002	0.9112
O	0.0014	−0.0016	0.9390
Mg	0.3357	0.6640	0.9696

References

1. Yum, J.H.; Nakade, S.; Kim, D.Y.; Yanagida, S. Improved performance in dye-sensitized solar cells employing TiO_2 photoelectrodes coated with metal hydroxides. *J. Phys. Chem. B* **2006**, *110*, 3215–3219. [CrossRef]
2. Nirmal Peiris, T.A.; Senthilarasu, S.; Upul Wijayantha, K.G. Enhanced performance of flexible dye-sensitized solar cells: Electrodeposition of $Mg(OH)_2$ on a Nanocrystalline TiO_2 electrode. *J. Phys. Chem.* **2011**, *116*, 1211–1218.
3. Huang, C.H.; Jan, Y.L.; Lee, W.C. Investigation of Mg(O,OH) films prepared by chemical bath deposition as buffer layer for Cu(In,Ga)Se_2 solar cell. *J. Electrochem. Soc.* **2011**, *158*, H879–H888. [CrossRef]
4. Miyazaki, H.; Mikami, R.; Yamada, A.; Konagai, M. Chemical-bath-deposited ZnO and $Mg(OH)_2$ buffer layer for Cu(InGa)Se_2 solar cells. *Jpn. J. Appl. Phys.* **2006**, *45*, 2618–2620. [CrossRef]
5. Kumari, L.; Li, W.Z.; Vannoy, C.H.; Leblanc, R.M.; Wang, D.Z. Synthesis, characterization and optical properties of $Mg(OH)_2$ micro-/nanostructure and its conversion to MgO. *Ceramics Int.* **2009**, *35*, 3355–3364. [CrossRef]
6. Pishtshev, A.; Karazhanov, S.Z.; Klopov, M. Materials properties of magnesium and calcium hydroxides from first-principles calculations. *Comp. Mater. Sci.* **2014**, *95*, 693–705. [CrossRef]
7. Li, T.; Ichimura, M. Fabrication of transparent $Mg(OH)_2$ thin films by drop-dry deposition. *Materials* **2021**, *14*, 724. [CrossRef] [PubMed]
8. Keikhaei, M.; Ichimura, M. n-type and p-type semiconducting Cu-doped Mg $(OH)_2$ thin films. *Semicond. Sci. Technol.* **2020**, *35*, 035020. [CrossRef]
9. Keikhaei, M.; Ichimura, M. Fabrication of $Mg(OH)_2$ Thin Films by Electrochemical Deposition with Cu Catalyst. *Thin Solid Films* **2019**, *681*, 41–46. [CrossRef]
10. Kang, J.; Keikhaei, M.; Li, T.; Ichimura, M. Galvanostatic electrochemical deposition of Cu-doped $Mg(OH)_2$ thin films and fabrication of p-n homojunction. *Mater. Res. Bull.* **2021**, *137*, 111207. [CrossRef]
11. Ichimura, M. Impurity doping in $Mg(OH)_2$ for n-type and p-type conductivity control. *Materials* **2020**, *13*, 2972. [CrossRef] [PubMed]
12. Wu, S.; Senevirathna, H.L.; Weerasinghe, P.V.T.; Wu, P. Engineering Electronic Structure and Band Alignment of 2D $Mg(OH)_2$ via Anion Doping for Photocatalytic Applications. *Materials* **2021**, *14*, 2640. [CrossRef] [PubMed]
13. Honjo, T.; Chiba, M.; Kuji, T. Novel rare-elements free transparent conductor of $Mg(OH)_2$-C compounds. *E J. Surf. Sci. Nanotechnol.* **2009**, *7*, 791–794. [CrossRef]

14. Guo, S.; Yang, L.; Dai, B.; Geng, F.; Yang, Z.; Wang, P.; Gao, G.; Lei, P.; Han, J.; Ralchenko, V.; et al. Wide-range infrared transparency of hydrated magnesium-carbon films with high mobility for enhanced conductivity. *Surf. Coat. Technol.* **2019**, *365*, 70–75. [CrossRef]
15. Kraut, E.A.; Grant, R.N.; Waldrop, J.R.; Kowalczyk, S.P. Precise Determination of the Valence-Band Edge in X-Ray Photoemission Spectra: Application to Measurement of Semiconductor Interface Potentials. *Phys. Rev. Lett.* **1980**, *44*, 1620–1623. [CrossRef]
16. Nelson, A.J.; Schwerdtfeger, C.R.; Wei, S.H.; Zunger, A.; Rioux, D.; Patel, R.; Höchst, H. Theoretical and experimental studies of the ZnSe/CulnSe, heterojunction band offset. *Appl. Phys. Lett.* **1993**, *62*, 2557–2559. [CrossRef]
17. Nelson, A.J. Photoemission study of CdS heterojunction formation with binary selenide semiconductors. *J. Appl. Phys.* **1995**, *78*, 5701–5705. [CrossRef]
18. Katnani, A.D.; Margaritondo, G. Microscopic study of semiconductor heterojunctions: Photoemission measurement of the valance-band discontinuity and of the potential barriers. *Phys. Rev. B* **1983**, *28*, 1944–1956. [CrossRef]
19. Bacaksiz, C.; Dominguez, A.; Rubio, A.; Senger, R.T.; Sahin, H. h-AlN-$Mg(OH)_2$ van der Waals bilayer heterostructure: Tuning the excitonic characteristics. *Phys. Rev. B* **2017**, *95*, 075423. [CrossRef]
20. Ren, K.; Yu, J.; Tang, W. A two-dimensional vertical van der Waals heterostructure based on g-GaN and $Mg(OH)_2$ used as a promising photocatalyst for water splitting: A first-principles calculation. *J. Appl. Phys.* **2019**, *126*, 065701. [CrossRef]
21. Yagmurcukardes, M.; Torun, E.; Senger, R.T.; Peeters, F.M.; Sahin, H. $Mg(OH)_2$-WS_2 van der Waals heterobilayer: Electric field tunable band-gap crossover. *Phys. Rev. B* **2016**, *94*, 195403. [CrossRef]
22. Ren, K.; Yu, J.; Tang, W.C. First-principles study of two-dimensional van der Waals heterostructure based on ZnO and $Mg(OH)_2$: A potential photocatalyst for water splitting. *Phys. Lett. A* **2019**, *383*, 125916. [CrossRef]
23. Császár, P.; Pulay, P. Geometry optimization by direct inversion in the iterative subspace. *J. Mol. Struct.* **1984**, *114*, 31–34. [CrossRef]
24. Hohenberg, P.; Kohn, W. Inhomogeneous Electron Gas. *Phys. Rev.* **1964**, *136*, B864–B871. [CrossRef]
25. Kohn, W.; Sham, L.J. Self-Consistent Equations Including Exchange and Correlation Effects. *Phys. Rev.* **1965**, *140*, A1133–A1138. [CrossRef]
26. Perdew, J.P.; Burke, K.; Ernzerholf, M. Generalized Gradient Approximation Made Simple. *Phys. Rev. Lett.* **1996**, *77*, 3865–3867. [CrossRef]
27. Janotti, A.; van de Walle, C.G. Absolute deformation potentials and band alignment of wurtzite ZnO, MgO, and CdO. *Phys. Rev. B* **2007**, *75*, 121201. [CrossRef]
28. Harun, K.; Salleh, N.A.; Deghfel, B.; Yaakob, M.K.; Mohamad, A.A. DFT + U calculations for electronic, structural, and optical properties of ZnO wurtzite structure: A review. *Results Phys.* **2020**, *16*, 102829. [CrossRef]
29. Perdew, J.P.; Yang, W.; Burke, K.; Yang, Z.; Gross, E.K.U.; Scheffler, M.; Scuseria, G.E.; Henderson, T.M.; Zhang, I.Y.; Ruzsinszky, A.; et al. Understanding band gaps of solids in generalized Kohn–Sham theory. *Proc. Natl. Acad. Sci. USA* **2017**, *114*, 2801–2806. [CrossRef]
30. Santamaria, M.; Di Quarto, F.; Zanna, S.; Marcus, P. Initial surface film on magnesium metal: A characterization by X-ray photoelectron spectroscopy (XPS) and photocurrent spectroscopy (PCS). *Electrochim. Acta* **2007**, *53*, 1315–1324. [CrossRef]
31. Hahn, R.; Brunner, J.G.; Kunze, J.; Schmuki, P.; Virtanen, S. A novel approach for the formation of $Mg(OH)_2$/MgO nanowhiskers on magnesium: Rapid anodization in chloride containing solutions. *Electrochem. Commun.* **2008**, *10*, 288–292. [CrossRef]
32. Klaua, M.; Ullmann, D.; Barthel, J.; Wulfhekel, W.; Kirschner, J.; Urban, R.; Monchesky, T.L.; Enders, A.; Cochran, J.F.; Heinrich, B. Growth, structure, electronic, and magnetic properties of MgO/Fe(001) bilayers and Fe/MgO/Fe(001) trilayers. *Phys. Rev. B* **2001**, *64*, 134411. [CrossRef]
33. Lany, S.; Osorio-Guillén, J.; Zunger, A. Origins of the doping asymmetry in oxides: Hole doping in NiO versus electron doping in ZnO. *Phys. Rev. B* **2007**, *75*, 241203. [CrossRef]
34. Minemoto, T.; Hashimoto, Y.; Satoh, T.; Negami, T.; Takakura, H.; Hamakawa, Y. Cu(In,Ga)Se_2 solar cells with controlled conduction band offset of window/Cu(In,Ga)Se_2 layers. *J. Appl. Phys.* **2001**, *89*, 8327–8330. [CrossRef]
35. Wang, M.; Yi, J.; Yang, S.; Cao, Z.; Huang, X.; Li, Y.; Li, H.; Zhong, J. Electrodeposition of Mg doped ZnO thin film for the window layer of CIGS solar cell. *Appl. Surf. Sci.* **2016**, *382*, 217–224. [CrossRef]
36. Tanaka, K.; Minemoto, T.; Takakura, H. Analysis of heterointerface recombination by $Zn_{1-x}Mg_xO$ for window layer of Cu(In,Ga)Se_2 solar cells. *Sol. Energy* **2009**, *83*, 477–479. [CrossRef]
37. Wong, L.M.; Chiam, S.Y.; Huang, J.Q.; Wang, S.J.; Pan, J.S.; Chim, W.K. Growth of Cu_2O on Ga-doped ZnO and their interface energy alignment for thin film solar cells. *J. Appl. Phys.* **2010**, *108*, 033702. [CrossRef]
38. Ichimura, M.; Song, Y. Band Alignment at the Cu_2O/ZnO Heterojunction. *Jpn. J. Appl. Phys.* **2011**, *50*, 051002. [CrossRef]
39. Duan, Z.; Du Pasquier, A.; Lu, Y.; Xu, Y.; Garfunkel, E. Effects of Mg composition on open circuit voltage of Cu_2O–$Mg_xZn_{1-x}O$ heterojunction solar cells. *Sol. Energy Mater. Sol. Cells* **2012**, *96*, 292–297. [CrossRef]
40. Minami, T.; Nishi, Y.; Miyata, T. High-Efficiency Cu_2O-Based Heterojunction Solar Cells Fabricated Using a Ga_2O_3 Thin Film as N-Type Layer. *Appl. Phys. Exp.* **2013**, *6*, 044101. [CrossRef]
41. Morales-Guio, C.G.; Tilley, S.D.; Vrubel, H.; Gr¨atzel, M.; Hu, X. Hydrogen evolution from a copper(I) oxide photocathode coated with an amorphous molybdenum sulphide catalyst. *Nat. Commun.* **2014**, *5*, 3059. [CrossRef] [PubMed]

42. Stevanovic, V.; Lany, S.; Ginley, D.S.; Tumas, W.; Zunger, A. Assessing capability of semiconductors to split water using ionization potentials and electron affinities only. *Phys. Chem. Chem. Phys.* **2014**, *16*, 3706–3714. [CrossRef] [PubMed]
43. Pan, H. Principles on design and fabrication of nanomaterials as photocatalysts for water-splitting. *Renew. Sustain. Energy Rev.* **2016**, *57*, 584–601. [CrossRef]